RSS Tech. Report 082702 **Issued: August 27, 2002**

Third Annual Progress Report: June 2001 through June 2002

Lower Tropospheric Air Temperature Derived from a Blended Analysis of MSU, SSM/T1, SSM/I, NCEP/NCAR Reanalysis, and Reynolds SST

NOAA Climate and Global Change Program
Joint NOAA/NASA Enhanced Data Set Project

Principal Investigator: Frank J. Wentz
Co-Investigators: Matthias Schabel & Carl Mears of RSS
Co-Investigator: Dian Seidel of NOAA Air Resources Lab

Submitted to:
Office of Global Programs
National Oceanic and Atmospheric Administration
1100 Wayne Avenue, Suite 1225
Silver Spring, MD 20910-5603

Submitted by:

Remote Sensing Systems
438 First Street, Suite 200, Santa Rosa, CA 95401
(707) 545-2904

I. Introduction

During the past year, Remote Sensing Systems has made significant progress in our climatological analysis of sounding data from the Microwave Sound Unit series of instruments. We have completed our reconstruction a single time series for MSU Channel 2 by combining data from the 9 satellite in the series, including developing a new model-based adjustment for drifts in the sampling of the diurnal cycle. Using the methodology we developed for Channel 2, we have also been able to produce precisely merged datasets for MSU Channels 3 and 4. Monthly mean brightness temperatures and anomalies are currently available on the RSS websites along with corresponding binary data.

Our first two reports focused on the development of quality control procedures, adjustments made to the data to account for variations in earth incidence angle caused by drifts and biases in spacecraft altitude and attitude, and preliminary attempts to adjust the data for drifts in the cycling of the diurnal cycle. The second report also gave a detailed description of the methodology we developed to merge the data from the nine distinct satellites into a single time series. In this report, we will provide an account of our new model-based method to account for the diurnal cycle, improvements in the merging procedure, and results we have obtained for MSU Channels 2, 3 and 4. After developing the merging and adjustment procedures for Channel 2, it proved to be relatively easy to extend them to lower stratosphere channel, Channel 4. Channel 3, which samples the upper troposphere/low stratosphere was also relatively easy to analyze, except that large and unexplained drifts in Channel 3 for both the NOAA-6 and NOAA-9 satellites make it impossible to recover climate quality data before December, 1986. These drifts were noticed previously noted by Spencer and Christy [1] and led them to choose to not produce a product for channel 3. Now, in 2002, enough time have passed since the advent of data from NOAA-10 in December of 1986 to make the production of a climate quality Channel 3 product a worthwhile exercise.

II. Diurnal Cycle Adjustment

Several of the MSU instruments exhibited significant drift in local equatorial crossing time (LECT). We show a time series of the LECT for each instrument in Fig. 1. Because of this drift, the instruments measure the properties of the atmosphere at local times which vary over each instrument's lifetime. If the temperature of the atmosphere or surface undergoes diurnal variations, this drift in sampling time can cause aliasing of the diurnal signal into the long-term time series, and possibly give rise to an artificial increase or decrease in the measured brightness temperatures (T_b's) that is unrelated to any long term trend in the atmospheric temperature. As we have noted in our previous reports, an important component of a climatological analysis of the MSU data is to account for these long term "diurnal" drifts. Spencer and Christy [4] accounted for these drifts by noting systematic differences between measurements made as the instrument

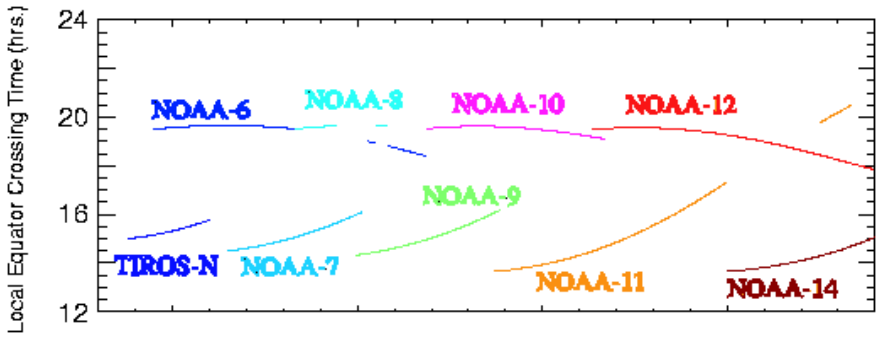

Fig. 1. Local equator crossing times (LECTs) for each satellite, showing the long-term drift in local observing time.

scanned across the satellite sub-track, and thus made measurements at different local time. When we duplicated this method, we found that it has the drawback that, due to sampling noise, zonal averages must be used to determine the slope of the diurnal cycle at a given measurement time accurately enough to perform the adjustment. This results in inaccuracies when the diurnal correction is used to produce a gridded map of decadal trends, since different locations within the same zonal band can have very different diurnal cycles. In this work, we use a new method based on a general circulation model, the NCAR community climate model (CCM3) [5] to calculate a five year climatology of local diurnal anomalies in the brightness temperature for each of the 6 cross-track view angles measured by the MSU instrument In collaboration with Ben Santer and Bala Govindasamy at the Program for Climate Model Diagnosis and Intercomparison, Lawrence Livermore National Laboratory, we performed a special analysis run of the CCM3 where the results for 5 years (1979-1984) were output on an hourly time scale. We choose to make a special run at this fine time scale to ensure that we clearly resolve the higher harmonics of the diurnal cycle. This is important for the following reason: typically, measurements from both the ascending and descending nodes are averaged together to make a final product. These measurements are separated in local time by about 12 hours for tropical and mid-latitude regions. This separation causes the effects of the first harmonic of the diurnal cycle to cancel, and the effects of the second harmonic to dominate. Standard model output is typically separated by 6 hours, and therefore is at the Nyquist frequency for the second harmonic, and does not define its properties.

A. DIURNAL BRIGHTNESS TEMPERATURE CLIMATOLOGY

The CCM3 model produces atmospheric temperature and humidity profiles and surface temperatures hourly on a 128 x 64 (T42) grid of earth locations. Each profile and surface temperature is used as input to our microwave radiative transfer and surface emissivity models [6] to calculate MSU channel 2 brightness temperature for each of the 6 distinct MSU view angles. For the oceans, we use a comprehensive surface model that includes the effects of wind-induced surface roughness and the variation of emissivity with sea surface temperature. For land, we assume a constant emissivity of 0.95. (This assumption for land is clearly an oversimplification, since the land emissivity can change dramatically with surface wetness and snow cover. We are currently working on refining our land surface emissivity model for a future analysis of MSU channel 1, where surface

effects will be more important.) This procedure results in a 5-year time series of brightness temperatures for each grid point and view angle. To produce a monthly climatology, the time series for each location is divided into months, and the mean diurnal anomaly for the specific location, month, and view angle is computed. We then resample the gridded climatology onto the 144 x 72 grid we use for representing the MSU data. By using microwave frequencies in our radiative transfer model we can simulate results for each of the MSU channels. We have done this for MSU Channels 2,3, and 4. The analysis of Channel 1 requires, as mentioned above, further refinements of our surface model to be useful in adjusting the MSU data.

In Fig. 2, we show four examples of the brightness temperature diurnal cycle anomalies calculated using the above methods for two locations on the earth, and for the nadir and near-limb view angles. In Fig. 2, (a) and (c), we show the diurnal cycles for a location in the equatorial Pacific for the nadir and near-limb view angles. Both show a similar diurnal cycle, indicating that the calculated diurnal cycle over the oceans is mostly due to warming in a thick layer of the atmosphere, and suggesting that near-surface warming is not important. Note that the lower boundary condition for the model over the ocean is a weekly sea surface temperature analysis that is constant on the diurnal time scale, so there will be no surface diurnal cycle in these data. The validity of this assumption is supported by sea surface temperatures retrieved from the TRMM Microwave Imager (TMI). These show very little diurnal variation (< 0.5K), except in regions of very low (< 3 m/s) wind speed [7], which occur rarely.

Fig. 2 (b) and (d) are for a location in the western United States. The land location, relatively dry atmosphere, and summer time period result in a large diurnal cycle in the simulated brightness temperature for channel 2. In contrast to (a) and (c), there is significant reduction in amplitude of the channel 2 near-limb view relative to the nadir view indicates that in this case, a significant portion of the MSU channel 2 diurnal cycle

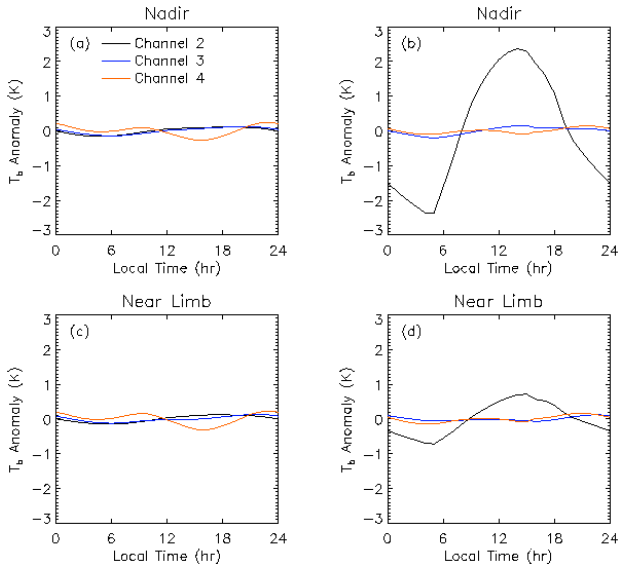

Fig. 2. Example simulated MSU diurnal cycles for channels 2,3 and 4 calculated from hourly CCM3 output. These diurnal cycles are for the month of June. (a) and (c) are for a 2.5 x 2.5-degree box in the tropical Pacific, centered at 178.75 W, 1.25 N. (b) and (d) are for a 2.5 x 2.5 degree box in the western United States., centered at 113.75 W, 38.75 N.

is due to surface warming. The surface signal is attenuated by the longer path through the atmosphere for the near-limb view. The diurnal cycles in channels 3 and 4 are much attenuated relative to channel 2, and are qualitatively similar to those found over the ocean for these channels.

In Figs. 3-5, we show maps of the diurnal amplitude and the local time of diurnal maximum for the month of June for the nadir view for channels 2,3, and 4. For channel 2, the simulated diurnal cycle has the largest amplitude in high altitude regions, where the surface is less obscured by atmospheric absorption, and in dry regions, which have large near-surface diurnal cycles due to night time radiative cooling. In the regions with the largest amplitudes, the brightness temperature peaks shortly after local noon, while land regions with smaller amplitudes peak a few hours later. Low- and mid-latitude ocean regions tend to peak even later in the day, though with much reduced amplitude. The spatial structure of the diurnal cycle for channels 3 and 4 is less correlated with surface type, except for the noticeable effects of the Tibetan Plateau in channel 3. The local time at diurnal maximum is complicated for channel 4 by double peaked, (semi-diurnal) behavior in the average diurnal cycles.

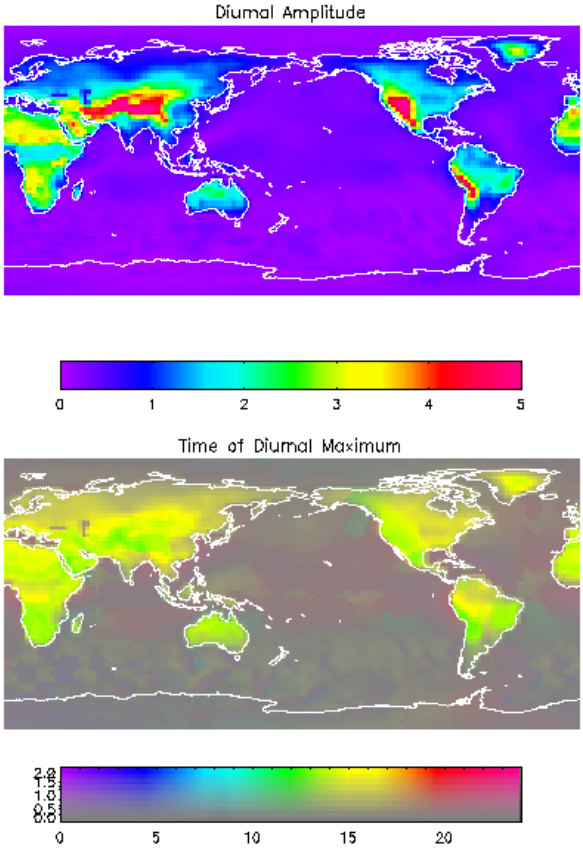

Fig. 3. (top) Mean simulated MSU Channel 2 diurnal amplitude for the June, nadir view. (bottom) Mean local time of simulated diurnal maximum, with the amplitude of the diurnal cycle denoted by the saturation of the color (this is done so the reader is not confused by anomalous diurnal maxima caused by noise in regions with a very small diurnal amplitude).

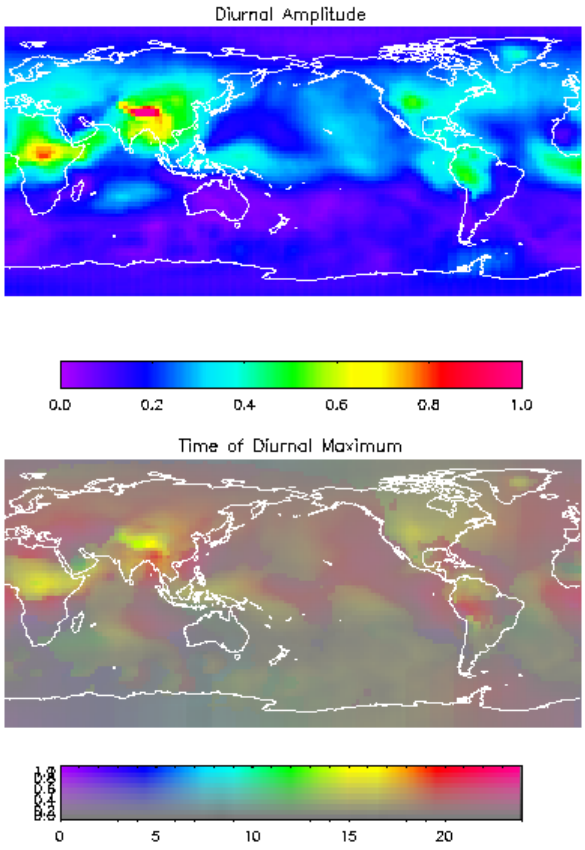

Fig. 4. (top) Mean simulated MSU Channel 3 diurnal amplitude for the June, nadir view. (bottom) Mean local time of simulated diurnal maximum, with the amplitude of the diurnal cycle denoted by the saturation of the color. Note the more sensitive ampltude scale relative to channel 2.

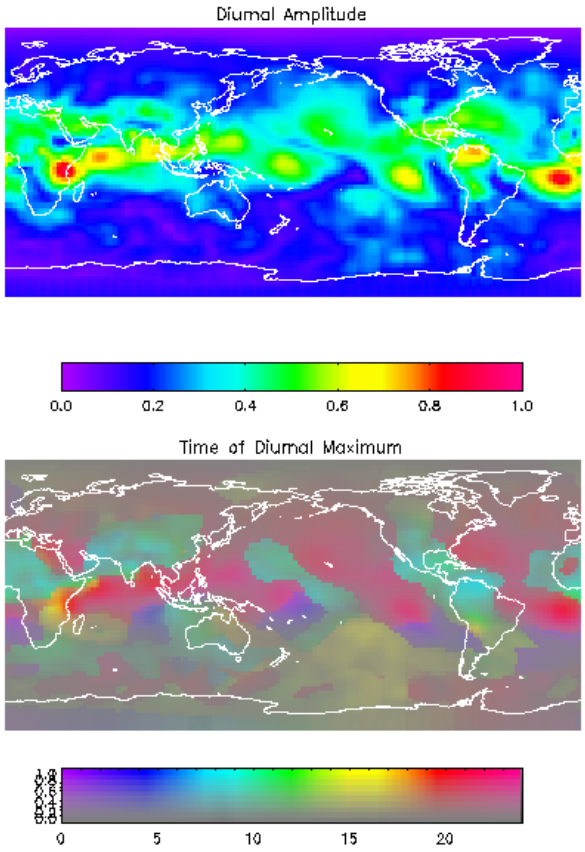

Fig. 5. (top) Mean simulated MSU Channel 4 diurnal amplitude for the June, nadir view. (bottom) Mean local time of simulated diurnal maximum, with the amplitude of the diurnal cycle denoted by the saturation of the color. The discontinuities in the diurnal maximum are due to the fact that often the channel 4 diurnal cycle exhibits 2 daily local maxima. The discontinuities occur at boundaries between regions where one or the other local maxima is the largest.

In Fig. 6, we plot three different mean diurnal cycle for each channel, corresponding to the global, land-only, and ocean-only averages. Data from each month are plotted separately. Only Channel 2 shows a significant difference between land and ocean. The double-peaked nature of the Channel 4 diurnal cycle that we mentioned above can also clearly be seen.

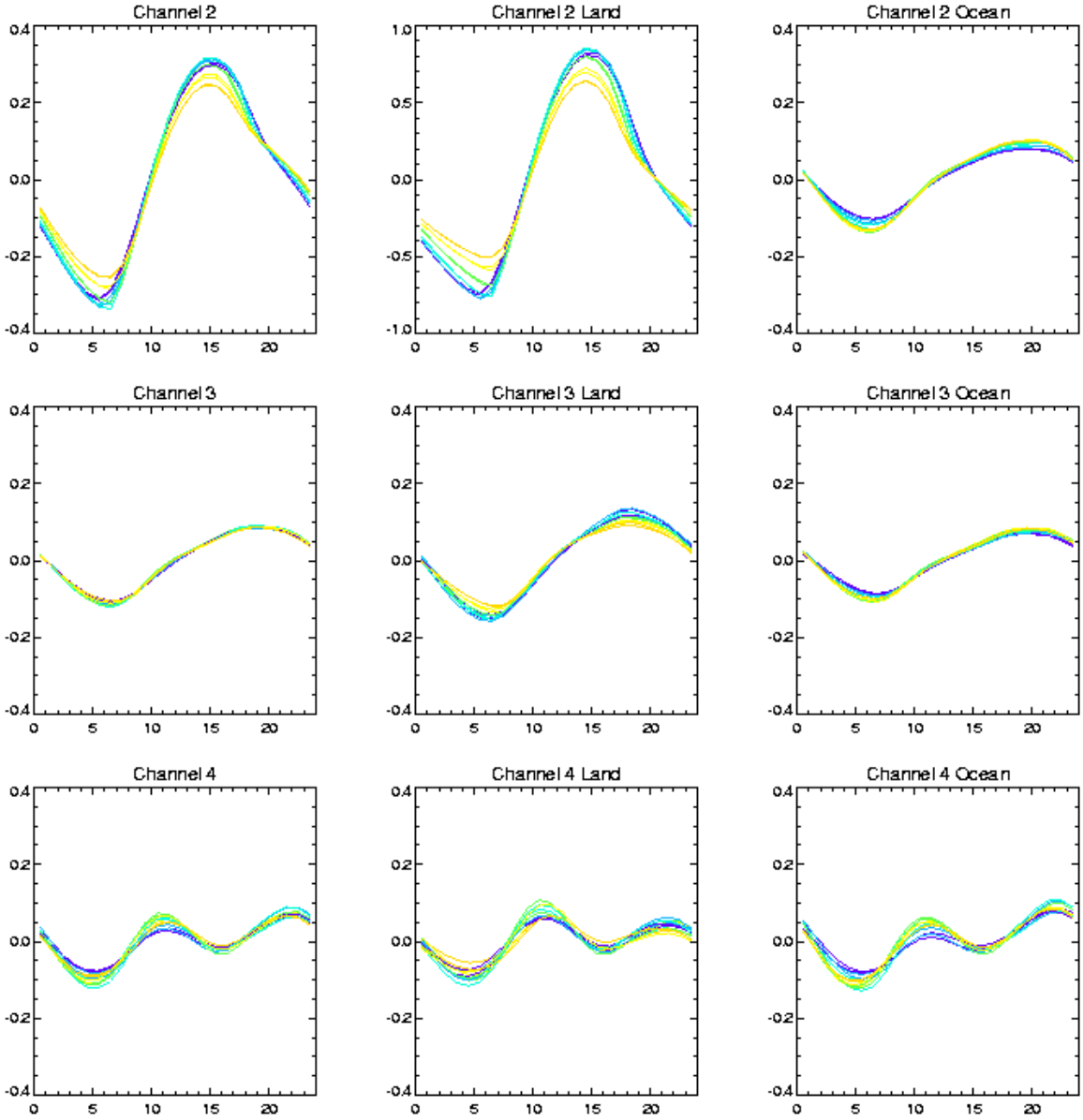

Fig. 6. Average global monthly diurnal cycles for the nadir view for each channel. We show the global average, as well as the global land and ocean averages. Northern hemisphere summers are shown in blue color, and winters in yellow colors. Channel 2 shows a significant difference between land on ocean that is not seen for channels 3 and 4. The channel 2 land diurnal cycle is much larger, and peaks earlier in the day than the ocean diurnal cycle. (Note the larger vertical scale for the channel 2 land plot). The double peaked nature of the channel 4 diurnal cycle is also easy to see.

C. VALIDATING THE CCM3-BASED DIURNAL CLIMATOLOGY.

Before using the above diurnal cycles to adjust long term time series of MSU brightness temperatures, we need to test its validity to the extent possible. To do this, we can use the measured MSU brightness temperatures. A straightforward way to do this that reduces the effects of long-term trends being aliased to the diurnal cycle is to compare ascending and descending measurements of the same earth location during the same time period. The difference between ascending and descending node measurements can be compared to similar differences calculated using the CCM3 simulated diurnal cycles. The ascending and descending measurements are separated by ~12 hours near the equator, declining to ~10 hours at 65 N or 65 S.

We have assembled monthly averages of ascending and descending MSU measurements, binned into hourly bins by the local equatorial crossing time for the ascending node. When the entire MSU data set is used, there is a significant amount of data in 5 time bins -- those centered at 14:30,15:30,16:30,19:30 and 20:30 local time.

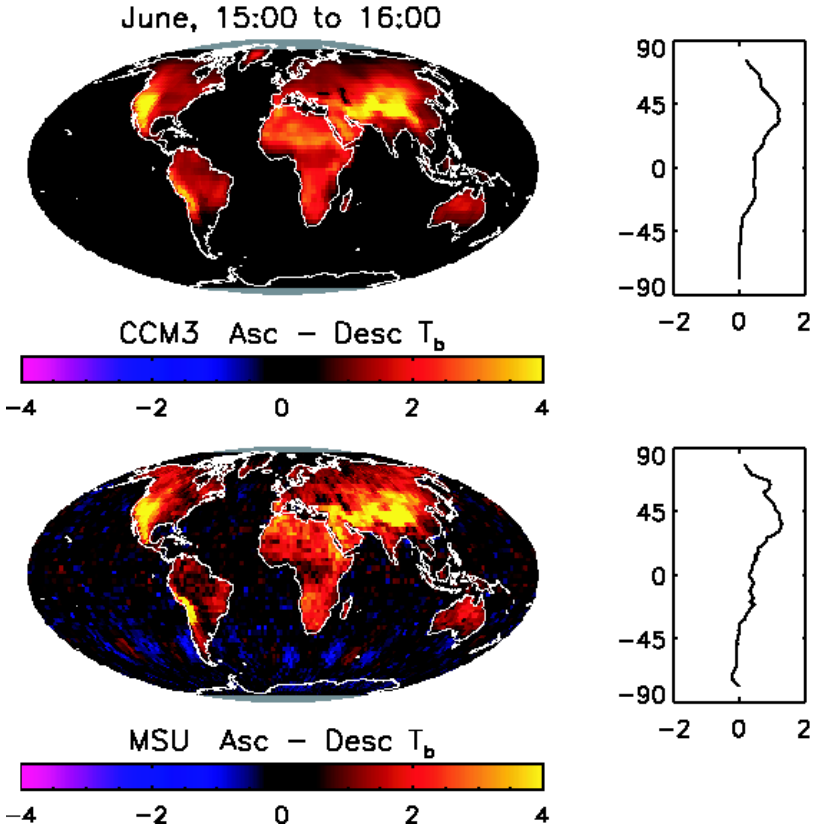

Fig. 7. Comparison of maps of the difference between the ascending and descending node MSU channel 2 brightness temperatures for the month of June, for ascending node equatorial crossing times between 15:00 and 16:00. The top map is the measured MSU channel 2 difference. The bottom map is the channel two difference simulated using the CCM3-derived diurnal climatology.

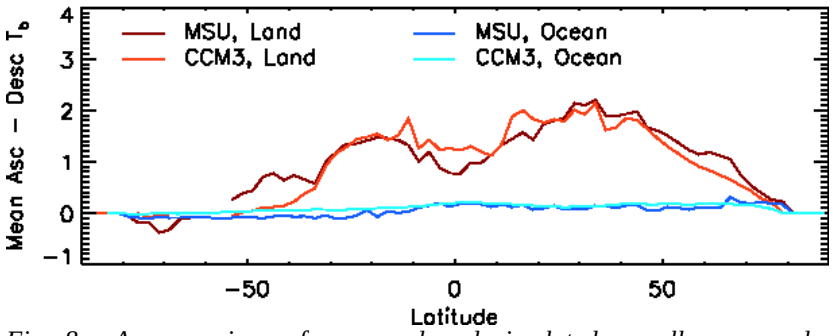

Fig. 8. A comparison of measured and simulated, zonally averaged ascending-descending differences for MSU channel 2. The ocean-only and land-only subsets are plotted separately.

The ascending and descending monthly averaged maps are then differenced for each crossing-time bin and we calculate maps of ascending-descending simulated brightness temperature differences with the same local (zonally dependent) observation times as the MSU difference. A comparison of these two sets of maps provides a validation of the diurnal variations simulated by CCM3. To reduce problems associated with sampling, we have combined the central 5 fields of view into a single map, after adjusting each measurement to the nadir view using our radiative transfer and surface models.

This procedure yields the best results for channel 2, due to its larger diurnal amplitude. In Fig. 7, we show as an example the comparisons between the measured and simulated ascend-descending differences for the 15:30 crossing-time bin for the month of June. We plot maps of the observed and simulated differences, and, in Fig. 8, a comparison of zonal averages for land and ocean separately. The agreement between the overall pattern and amplitude in most areas gives us confidence that the CCM3 model accurately represents MSU channel 2 diurnal cycle. The model appears to slightly overestimate the diurnal cycle over tropical forests (visible in tropical Africa and the Amazon Basin) and slightly underestimate the diurnal cycle in some high latitude land areas (visible in northwestern Canada and eastern Siberia). These discrepancies are not large enough to significantly change the diurnal correction applied to the MSU data.

Comparison of the ascending-descending difference for other crossing time bins and months show similar agreement, with the correlation coefficient between measured and simulated maps (spatially smoothed with a boxcar smooth of width 22.5 degrees to reduce sampling noise) remaining above 0.8 except for the crossing time bin centered at 20:30 local time. For this crossing time, the correlation coefficient is ~0.7 due to the increased relative importance of sampling noise since the signal amplitude has been reduced by approximately a factor of 4 for this later time.

The diurnal cycle for channels 3 and 4 has significantly less amplitude than for channel 2, making the spatial patterns in the diurnal cycle more difficult to see in the ascending/descending differences. This is particularly true for channel 4, where the diurnal cycle is dominated by semi-diurnal fluctuations, to which ascending-descending differences are not sensitive. For the early afternoon LECTs (14:00 – 17:00), sampling induced noise dominates the measured ascending descending differences. By the late afternoon LECTs, the ascending-descending differences have become large enough to see above the noise for a number of months. As an example, in Fig. 9 we show a pair of ascending-descending difference maps analogous to those in Fig 7, except for ascending

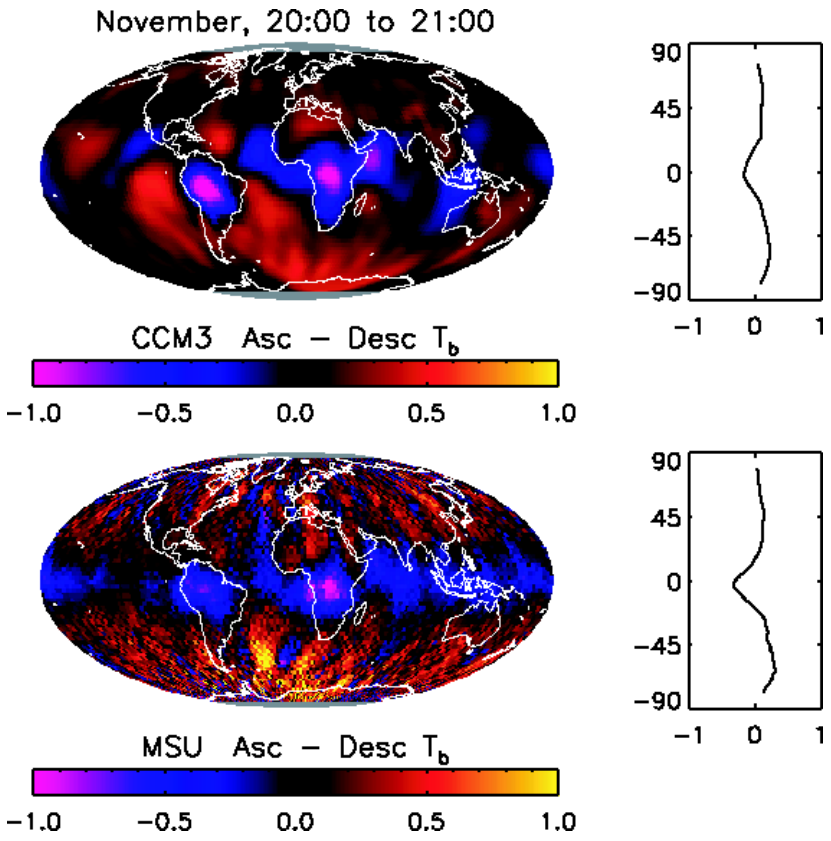

Figure 9. Ascending-Descending MSU channel 4 T_b differences for the month of November, for ascending times between 20:00 and 21:00.

LECTs between 20:00 and 21:00, for the month of November, and for channel 4. Noise dominates the measured map in many areas, but there is a large region of morning (descending) warmth over tropical South America and Africa that is also clearly seen in the CCM3 simulation. The zonal averages also agree quite well. The level of agreement in for channel 3 is about the same as we show here for channel 4.

We note that none of the validation done in this section directly validates the applied diurnal adjustments, since these are largely determined by the semi-diurnal part of the diurnal cycle, due to the ~12 hour difference in measurement time discussed above. However, these comparisons do give us confidence that the CCM3 model correctly simulates the overall amplitude of the diurnal cycle. A second validation of the diurnal cycle occurs when we find, in section III, that applying the CCM3 correction improves the quality of the intersatellite merges as measured by the r.m.s. average of the after the fit residuals.

D. Correction applied to the MSU time series

Using the diurnal climatology simulated using CCM3, we can adjust all MSU measurements to the same local time so that drifts in the measurement time no longer affect any deduced long term trends. The adjusted brightness temperature T_{Adj} is given by

$$T_{Adj} = T_{Meas} - T_{Sim}(t_{Meas}) + T_{Sim}(t_{Ref}).$$

Here, T_{meas} is the measured brightness temperature, $T_{Sim}(t)$ is the simulated diurnal anomaly at time t, t_{Meas} and t_{Ref} are the measurement and reference time. In practice, the simulated brightness temperatures are obtained by interpolating monthly gridded climatology both spatially and temporally. In Fig. 10, we plot the global correction applied to each time series for each satellite and channel to account for drifts in measurement time. The local reference time is chosen to be 12:00 noon for all satellites and both ascending and descending node. The choice of these times has little effect of the long term trends or intersatellite differences, since the effect of choosing a different time is to add the same periodic signal with a constant offset to all satellites.

The most important diurnal drift correction is that for NOAA-11, since this satellite underwent the largest drift in LECT during the time period shown, though the corrections for NOAA-7, NOAA-12 and NOAA-14 are also important. Depending on the techniques used to merge the time series for each satellite together, this diurnal correction increases the resulting global decadal trends by 0.02 to 0.05 K/decade, with the largest effect on trend over land for channel 2. The effect of the diurnal correction on channel 3 is minimal, due to its low amplitude and mostly sinusoidal shape.

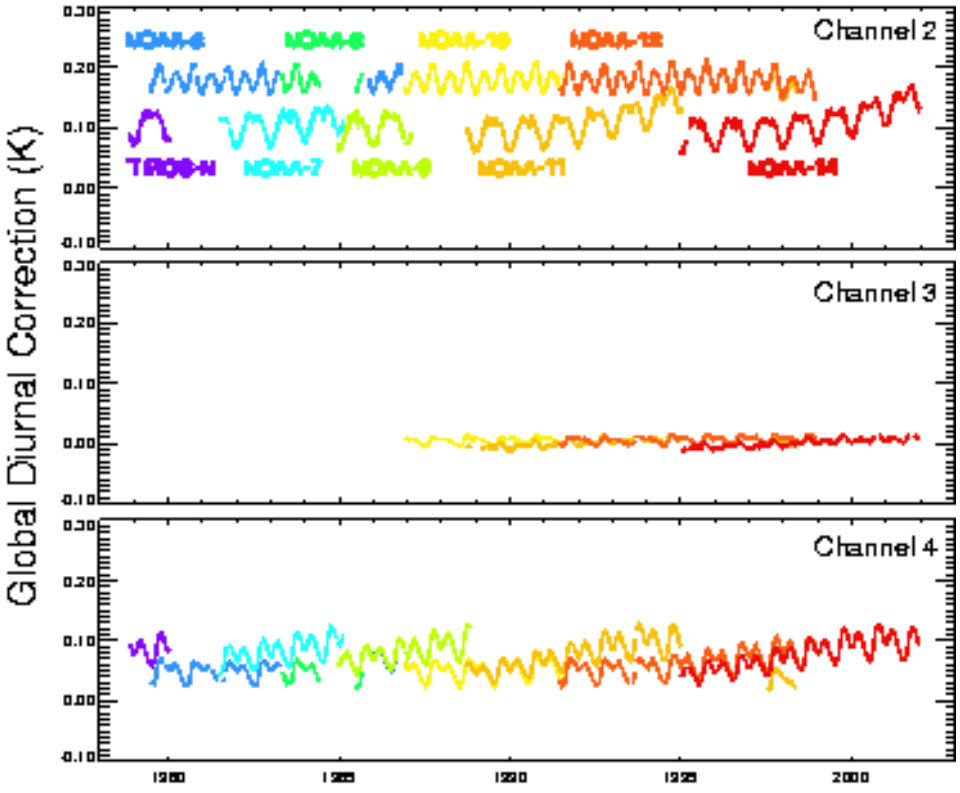

Fig. 10. Correction added to each time series to correct each measurement to local noon.

III. Merging

The method we use to merge the nine satellite into a single time series is discussed in detail in our progress report for 2001. After performing the altitude and attitude corrections outlined in the 2001 report, and the diurnal corrections discussed above, we assume that the remaining satellite errors are of the form

$$T_{MEAS,i} = T_0 + A_i + \alpha_i T_{TARGET,i} + \varepsilon_i ,$$

where the T_0 is the true brightness temperature, $T_{meas,i}$ is the temperature measured by the *ith* instrument, and $T_{TARGET,i}$ is the calibration target temperature., The A_i's are the intersatellite offsets, and the α_i's are the non-linearity factors (NLFs) that account for radiometer non-linearity, and ε_i is due to random noise.. We perform a linear regression to minimize the difference between contemporaneous measurements by co-orbiting satellites and to determine fitted values for the A_i's and α_i's. Corrected brightness temperatures are calculated by subtracting error terms from the measured values. These corrected temperatures can be averaged together to produce time series on a variety of temporal and spatial scales. In practice, we produce pentad and monthly global time series for the entire globe, ocean only measurements, and land only measurements, as well as monthly gridded time series on a 2.5 degree global grid. In the following sections, we discuss our results for each channel, and where appropriate, compare them with the earlier results of Christy and Spencer.

A. CHANNEL 2.

Channel 2 is the most complicated case of the 3 channels we have considered so far, due to the large diurnal cycle over dry land areas. Despite the validation efforts described above, we are still not completely confident in our diurnal corrections over land due to the simplicity of our assumptions about the land surface emissivity. For this reason, we choose to determine the NLFs for channel two by performing the merging regression using ocean-only observations, where the diurnal cycle is much smaller than for land. In Fig. 11 we summarize the merging procedure for ocean-only global pentad averages. In the top plot, we show the raw global, ocean-only brightness temperatures. In the middle plot, we show the intersatellite differences for cases where one or more satellites are observing for the same 5 day period, as well as the fit to these difference using the above model. We also show the residuals to the fit. In the bottom plot, we show the resulting merged time series anomaly, with the seasonal cycle removed, along with a linear fit.

It is clear that the error model accounts for almost all of the non-random differences between co-observing satellites. This gives us confidence that we have correctly determined the merging coefficients. A detailed error analysis (2001 progress report) determines the uncertainty in each coefficient, and the sensitivity of the decadal trend on these uncertainties. Most of the uncertainty is due to the offset and non-linearity coefficient for NOAA-9.

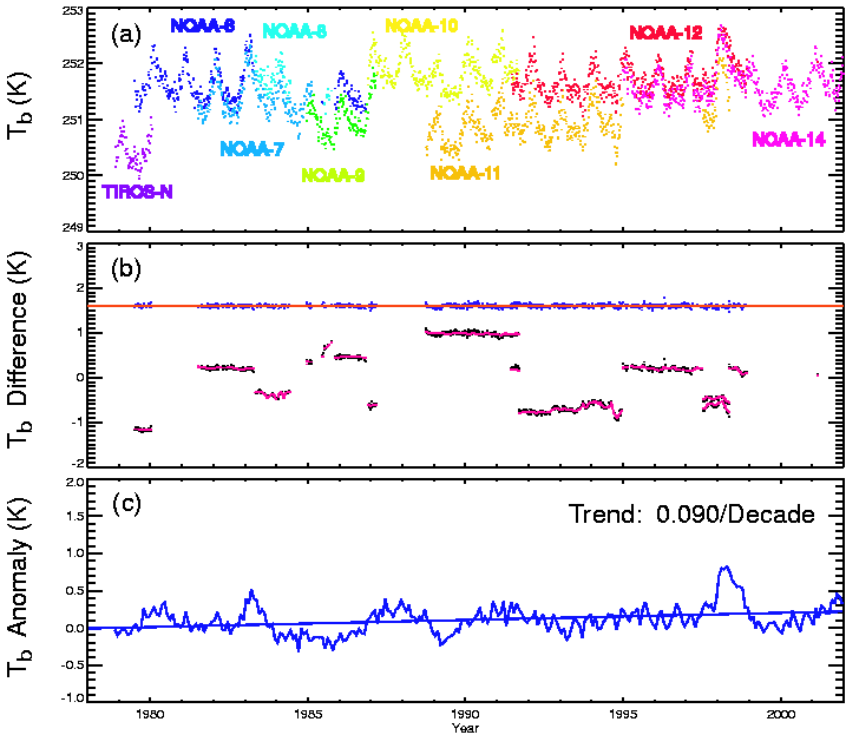

Fig. 11. Intersatellite merge using ocean-only Channel 2 data. (a) Unmerged pentad average of global, ocean-only channel 2 brightness temperatures. (b) black dots are the intersatellite differences, and the red lines are fits to these differences. The blue dots are the residuals to the fit. (c) brightness temperature anomaly with the seasonal cycle removed. The line is a linear fit to the anomalies.

Our next step is to perform the merge for the land-only subset. This land subset is interesting because the diurnal cycle is the largest over land, and hence the land-only merge is most sensitive to errors in the diurnal drift adjustment. In Fig. 12, we show the land-only merging process for the NOAA-11 – NOAA-12 overlap. During the 1991-1995 period of overlap between these two instruments, the ascending LECT for NOAA-11 drifted from 3:00 pm, just after the peak of the diurnal cycle, to 5:30, after significant diurnal cooling has occurred. NOAA-12 drifted little during this time period. The temperatures measured during the descending pass for NOAA-11 probably varied little, due to the early morning time of this pass. The effect of the drift is significant reduction of the NOAA-11 global averages during this time period relative to NOAA-12, which gives rise to the slope in the residuals that can be clearly seen in Fig. 12 (a).

When we repeat the calculation using data corrected for the diurnal cycle using the correction outlined in Section 3, we obtain the results shown in Fig. 12(b). The NOAA-11-NOAA-12 slope during 1991-1995 is mostly eliminated. The are two less significant features that remain. First, the residuals for the NOAA-11-NOAA-12 overlap in 1997-1998 are now slightly positive, suggesting that we may have applied slightly too much correction to these measurements. Second, there remain significant seasonal-scale oscillations in the NOAA-11—NOAA-12 residuals (though these too, are reduced by the correction). These seasonal scale fluctuations are somewhat troubling, since they would, if they are present, be difficult to observe in the short but critical overlap between

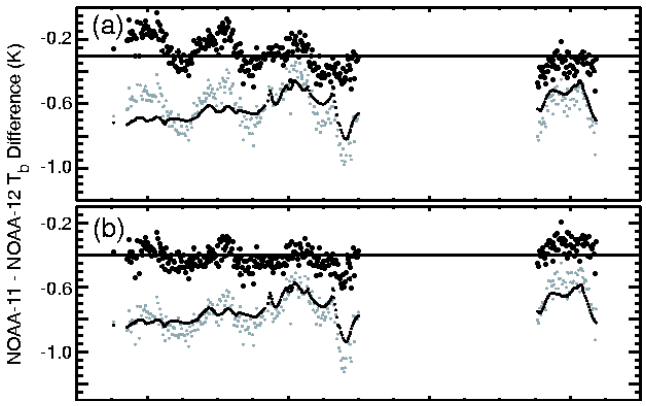

Fig. 12. Results of the satellite merging calculation analogous for the NOAA-11/NOAA-12 overlap period. The gray dots are the NOAA-11/NOAA-12 differences. The black dots represent the fit to the differences using the ocean-only NLFs. The black crosses are the after the fit residuals, offset so that the horizontal line is zero. (a) Merge performed without the diurnal correction. Note the overall slope of the residuals in the 1992-1995 time period due to the drift in local crossing time of NOAA-11. (b) Merge performed using the diurnal correction. Note the marked reduction in the slope, and to a lesser extent, the seasonal cycle in the residuals. This provides another check on the validity of the CCM3-based diurnal correction.

NOAA-9 and NOAA-10 and could lead to errors in this part of the overlap. These fluctuations are, however, only important for the land only merge. We shall see below that they are small for the global land-and-ocean merge. In Fig. 13 we plot the resulting global land-only anomaly time series. This time series shows a slightly larger warming trend than the ocean only trend.

We now perform a combined merge for global, land-and-ocean pentad averages. In Fig. 14, we show a summary of the merging process, similar to Fig. 11, except for global pentads. The non-linearity factors are set to the ocean-only values found above. The fit to the intersatellite differences again is able to remove almost all of the non-random fluctuations in the residuals to the fit, giving us confidence in our choice to use the ocean-only non-linearity factors. The T_b's show a significantly larger seasonal cycle, and are thus plotted on a difference scale. This anomaly time series, with the seasonal cycle

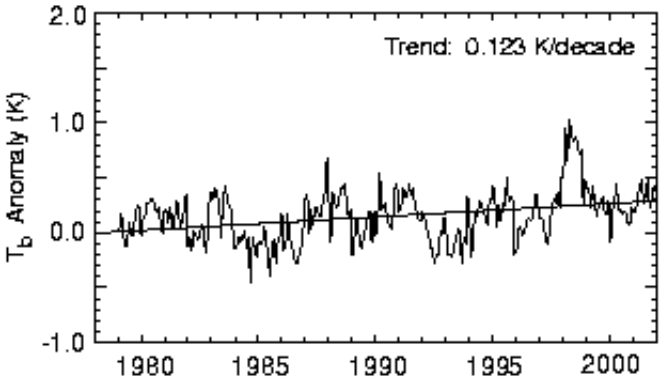

Fig 13. Land-Only, Global MSU channel 2 time series.

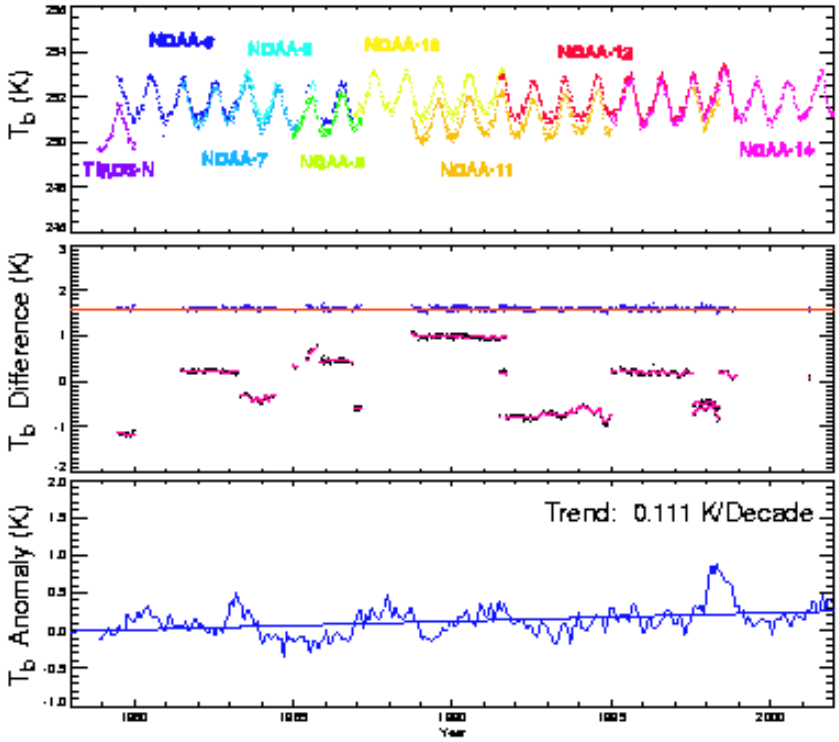

Fig 14. Same as Figure 11, except for land-and-ocean global pentads.

removed, shows warming of 0.111 +/- 0.020 K/decade, in between the ocean-only and land-only results as we might expect. The stated uncertainty is the 2-σ uncertainty due to the correlated errors estimated for the merging coefficients. The procedure used to calculate this uncertainty is discussed in detail in the 2001 progress report. This 2-σ uncertainty will be used for channels 3 and 4 also.

Since there was some indication in the land-only merge that we have overcorrected for the diurnal cycle, we have performed a study in which we vary the amount of diurnal correction applied, and note the amount that minimizes the standard deviation of the residuals. The results of this study are summarized in Fig. 15, where we plot the overall standard deviation of all the residuals to the land-and-ocean fit, and the standard deviation of residuals to the NOAA-11 – NOAA-12 overlap, as a function of a multiplicative diurnal adjustment factor that modifies the applied adjustment. For both cases we find a minimum at a value of about 0.9. This, combined with a similar indication in section II.C, leads us to conclude that the CCM3 channel 2 diurnal correction is about slightly too large. Also in Fig. 15, we plot the resulting global decadal trend as a function of the diurnal adjustment factor. Choosing a value of 0.9 reduces the resulting trend to about 0.100 +/- 0.020. From this point forward in this report, we will use a diurnal correction factor of 0.9 to slightly reduce the diurnal adjustment for channel 2.

Global map of anomalies and anomaly trends are useful for evaluating regional trends and comparing with model output. We have calculated monthly anomaly maps on a 2.5 by 2.5 degree scale for the entire MSU channel 2 dataset. The merging parameters were

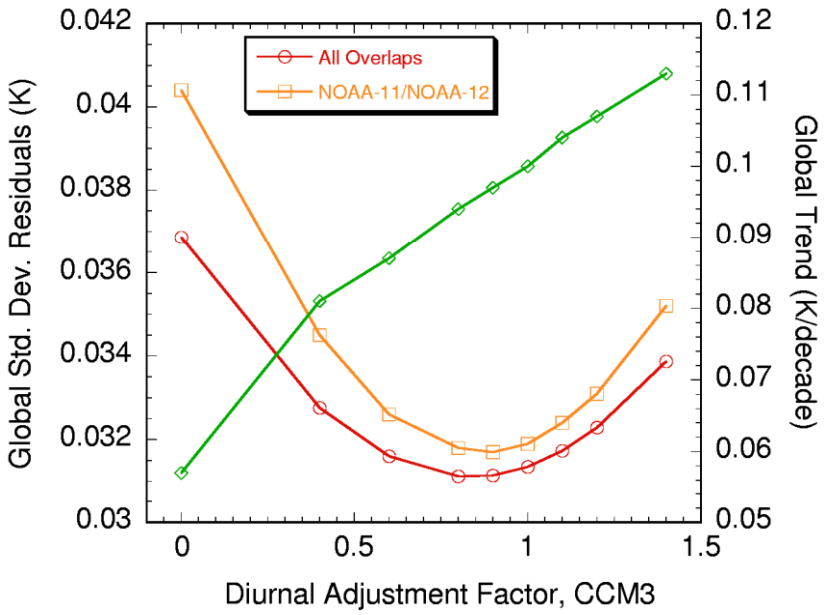

Fig. 15. Impact of varying the amount of diurnal correction applied. We plot the standard deviation of the after the fit residuals as a function of a multiplicative factor applied to the diurnal adjustment. Both the overall standard deviation, and that of the NOAA-11 – NOAA-12 overlap are minimized near 0.9. For reference, we also plot the Global trend found using varying amounts of diurnal adjustment

held constant for all locations; we used the ocean-only NLFs, and offsets derived during the land and ocean analysis presented in the section above. Using these monthly anomaly maps, we calculated a global trend map, which we show in Fig. 16. The map shows a large regions of significant warming over eastern and central Asia, and northern Canada, cooling over the southern oceans, with moderate warming over most other regions.

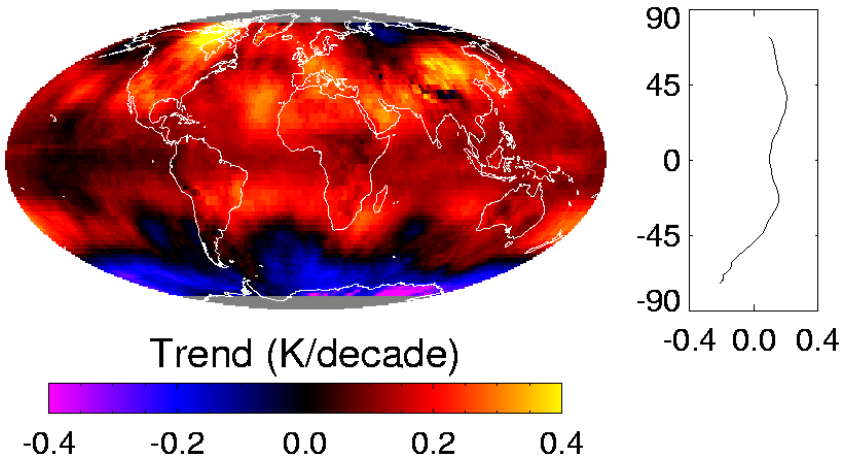

Figure 16. Color-coded map of global MSU channel 2 brightness temperature trends, 1979-2001.

B. CHANNEL 3.

We now move on to discuss out merging of measurements from MSU channel 3. We found the merging procedure for channel 3 to be much simpler than for channel 2 mostly because the weighting function for this channel peaks much higher in the atmosphere. This reduces the effects of surface to the extent that its no longer necessary to separate

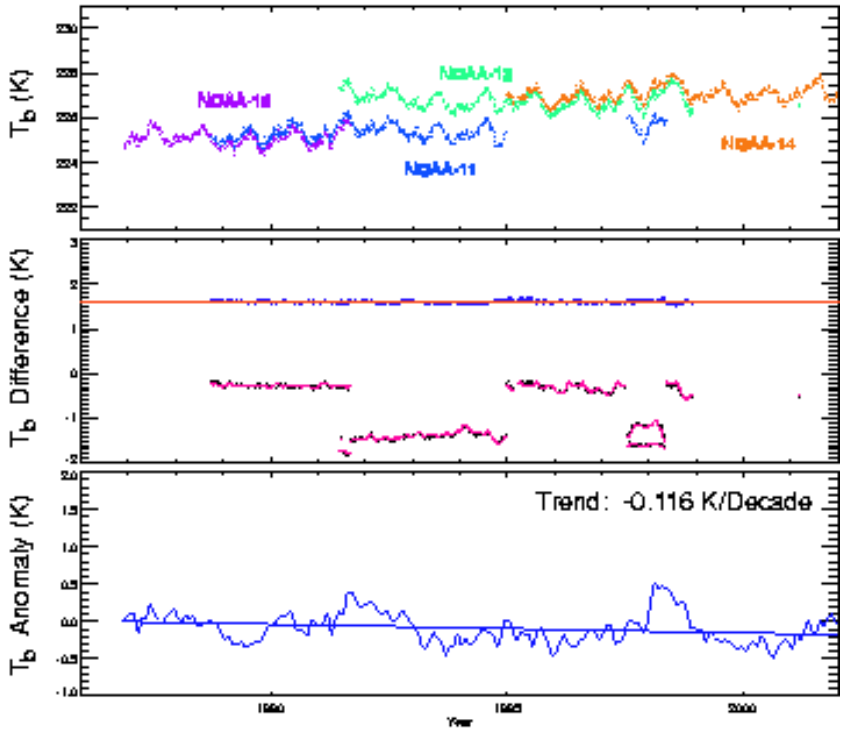

Fig 17. Summary of the merging procedure for channel 3. Large drifts in data from NOAA-6 and NOAA-9 preclude analysis for the time period before the advent of NOAA-10.

the land and ocean measurement. Also, we found that the diurnal cycle is much less important than for channel 2. Using the same error model that we use to perform the channel 2 merges, we discovered that both NOAA-6 and NOAA-9 exhibited large drifts that are uncorrelated with the calibration target temperature or local observing time, and are thus not removed by our procedure. This makes it impossible (for now) to retrieve an accurate merged brightness temperature before the beginning of valid data for NOAA-10 in December, 1986. We show a summary of the merging calculation for channel 3 of Fig. 17. Again, we find that the inclusion of the calibration target temperatures via the NLFs is necessary to remove seasonal-scale fluctuations in the intersatellite differences, leading to a decadal scale cooling trend of –0.116 +/- 0.012 K/decade. The interpretation of this trend is complicated, since the MSU channel 3 weighting function includes large contributions from both the upper troposphere (which may be warming), and the lower stratosphere (which is almost certainly cooling). In Fig 18, we show a map of channel 3 trends from 1987-2001. Note that this channel shows moderate warming in the equatorial regions, and cooling over the mid-latitude and polar regions. Cooling is strongest over the south pole.

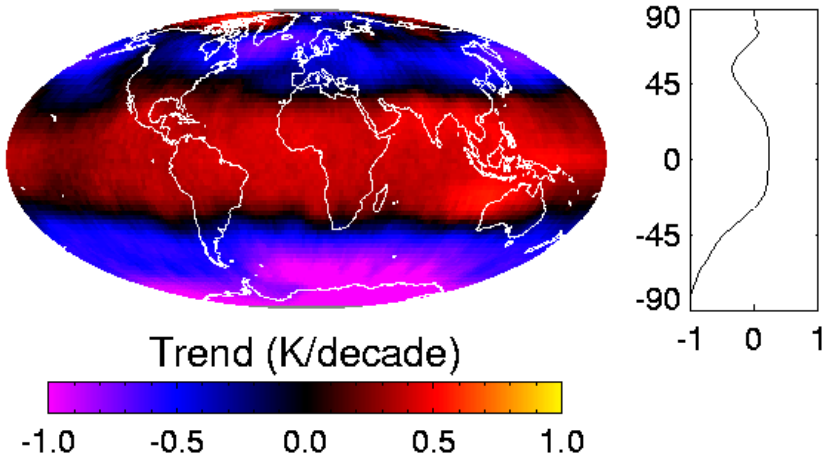

Fig. 18. Color-coded map of global MSU channel 3 brightness temperature trends, 1987-2001.

C. CHANNEL 4

Channel 4 is also relatively straightforward in comparison with channel 2. The main complication for channel 4 is the presence of a moderate diurnal cycle due to diurnal stratospheric tides. The diurnal signal is dominated by a semidiurnal signal, which, unlike the diurnal-mode-dominated channel 2, does not cancel when the ascending and descending nodes are combined, making its removal from channel 4 important. A variational analysis of the diurnal adjustment we apply, similar to that shown in Fig. 15, indicates that our diurnal cycle is of the correct magnitude and approximately the correct shape, and thus does not need an empirical adjustment factor.

When we perform the merging procedure for these data, again most of the seasonal scale fluctuations are accounted for by the fit. We believe that this is the first time a merge has been done for channel 4 that takes into account the target temperature dependence. The use of the non-linearity parameters increases the global by about 0.075 K/decade relative to the offset-only merged data.. The after the fit residuals show a higher level of noise (standard deviation = 0.042 K, compared to 0.032 K for channel 2). A similar effect is seen by Christy and Spencer. In Fig. 19, we summarize the merging procedure in the same format as Fig. 14. We find a decadal trend of –0.390 +/- 0.012 K/decade.

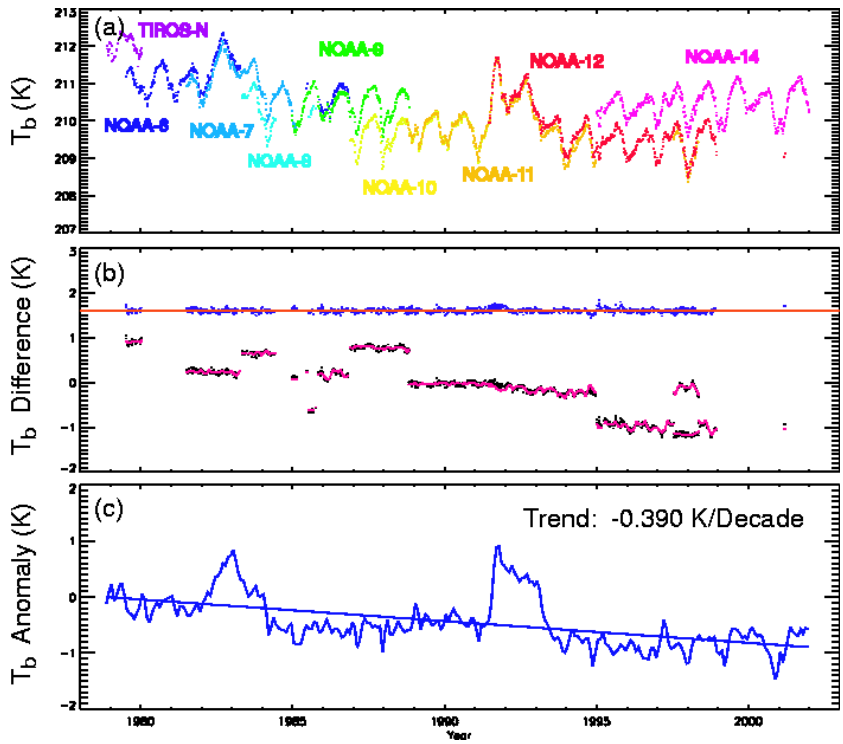

Fig. 19. Summary of Channel 4 Merging procedure. After the fit residuals are slightly larger than for channels 2 and 3. The anomaly time series shows a large cooling signal, punctuated bydramitic warming events caused by the eruptions of El Chichon (1982) and Mt. Pinatubo (1991).

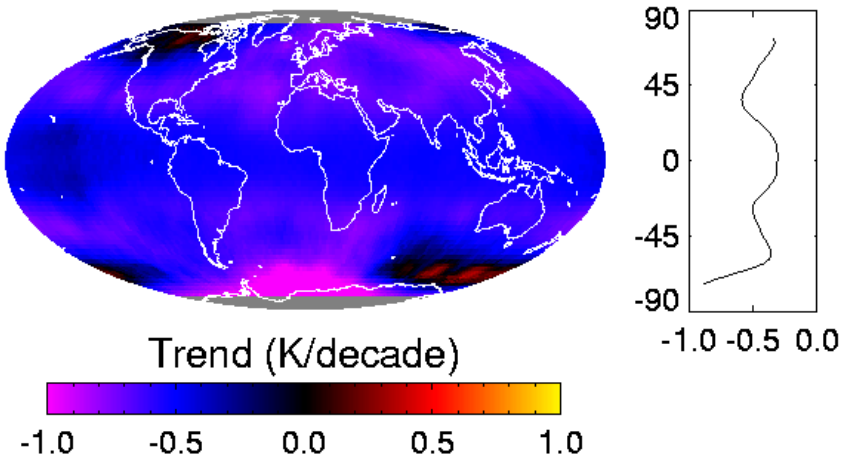

Fig. 20. Color-coded map of Channel 4 decadal trends

In Fig. 20, we show a color-coded map of channel 4 decadal trends for the time period 1979-2001. The entire globe shows cooling, except for a small region of warming over the southern oceans.

D. Availability of Data to the Scientific Community

We have made our gridded monthly data sets for MSU channels 2,3, and 4 available to a via our MSU website, http://www.remss.com/MSU/, along with reading routines for a variety of computer languages and analysis packages. We have also developed a simple web interface that allows users to browse through monthly maps of brightness temperature or brightness temperature anomaly data. In Fig. 21, we show a screen shot of our MSU web interface. We also include links to other useful information, such as vertical weighting functions for each channel to help interested researchers compare our products to model output or *in situ* data. After publishing a peer-reviewed paper documenting the data set for a given channel, we plan to make the data available to the National Climate Data Center (NCDC) for further dissemination.

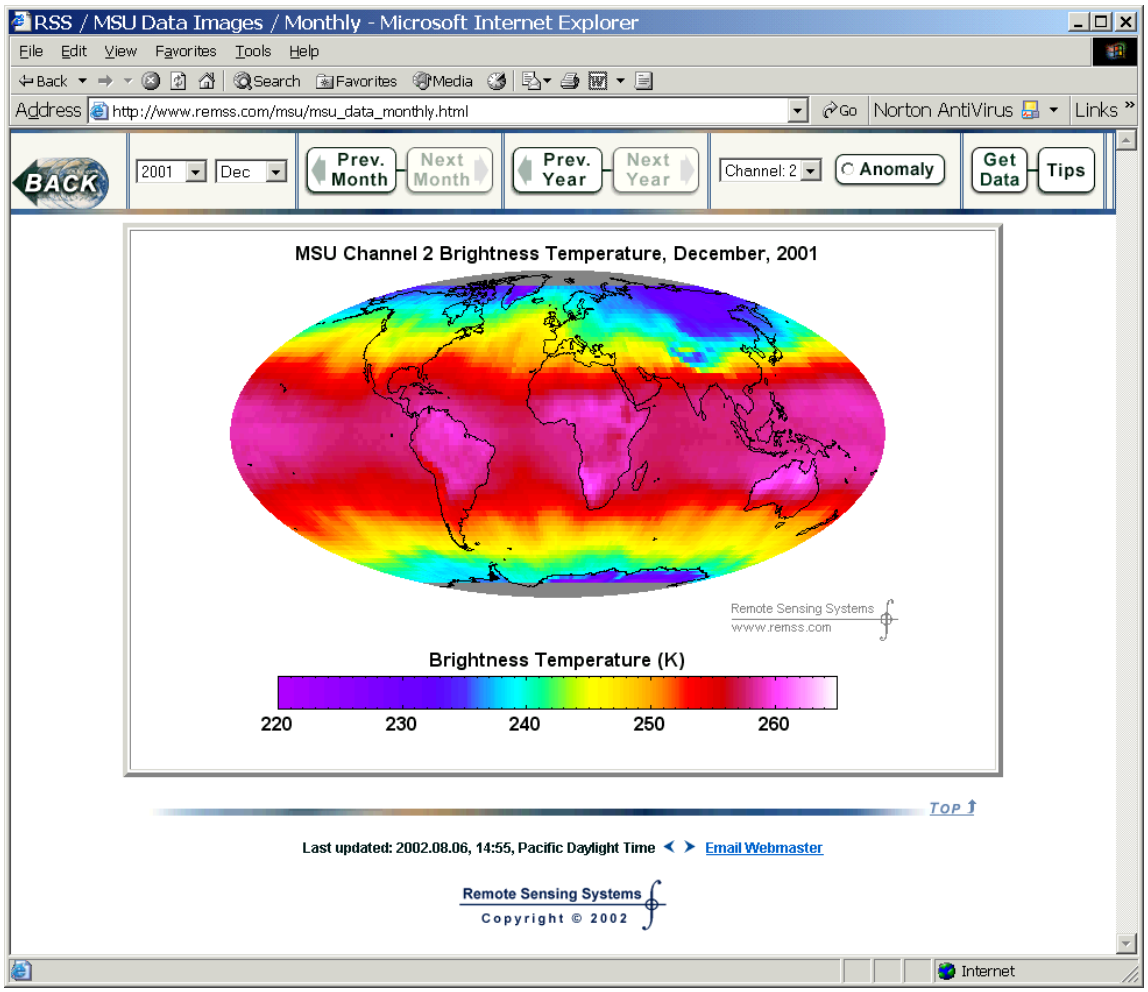

Fig. 21. Screen shot of our MSU web interface which allows users to browse through monthly maps of brightness temperature or brightness temperature anomaly to look for interesting events.

IV. Comparison with the previous results of Christy and Spencer

In this section, we compare our current results with previous results published by Christy and Spencer (C&S) for MSU Channels 2 and 4, and attmept to clarify the origin of discrepancies between their results and ours.

A. Channel 2

Our most controversial result is likely to be the long-term trend for MSU channel 2. In Fig. 21, we plot the anomaly time series for channel 2 determined by C&S together with our anomaly time series. Our new time series shows about 0.090 K/decade more warming than found by C&S. We also show the difference time series, which reveals two regions where our time series changes relative to the S&C time series. The first of these regions is a ramp that occurs from 1985 to 1987, during the lifetime of NOAA-9, the second is a slow ramp that occurs over a time period from 1991 to 1995, during when the LECT for NOAA-11 was drifting dramatically. The effect of these two regions of change is to yield decadal trends that are significantly different, as we summarize in Table 1

TABLE 1
GLOBAL TRENDS (K/DECADE)

	RSS	C&S
MSU 2	0.106 +/- 0.010	0.015
MSU 3	-0.116 +/-0.012	-
MSU 4	-0.390 +/-0.012	-0.505

The reported uncertainty is a 2-σ error, calculated using the Monte Carlo procedure in our previous progress report. Note there is a significant disagreement between our trends and those found using anomalies calculated by Christy and Spencer.

We find that this difference is due mostly to a difference between our value for the

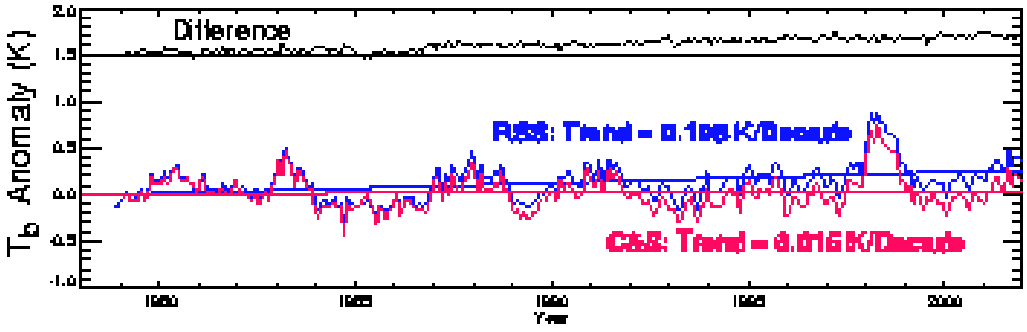

Fig. 22. Comparison of MSU Channel 2 global Time series. Our result shows approximately 0.090 K decade more warming than the C&S results for the same time period. Note the significant step in the difference time series in the 1985-1987 time period. This is the operation time period for NOAA-9.

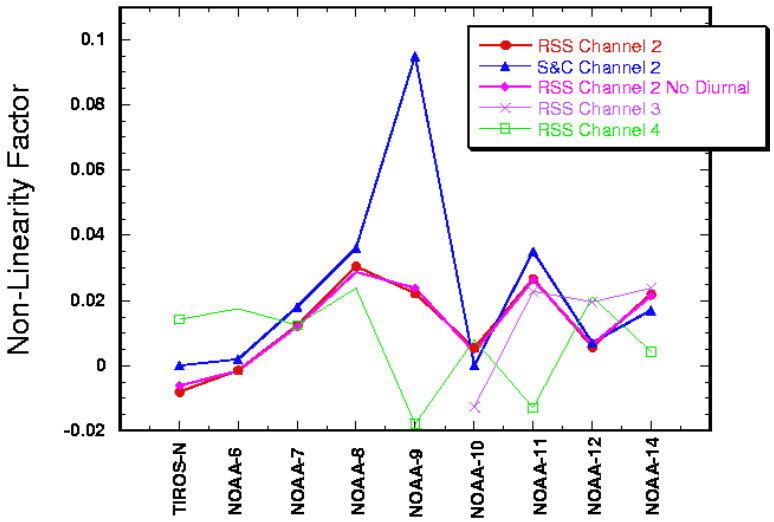

Fig. 23. Comparison of Non-linearity Factors (NLFs) for each satellite and channel. C&S's value for NOAA-9 is a clear outlier. RSS Channel 2 No Diurnal refers to the case where the merging regression was done without performing the diurnal adjustments.

NOAA-09 NLF and that used by C&S. In Fig 22, we plot the NLFs for all satellites for two versions of our analysis, and those used by Christy and Spencer[4]. For reference, we also include the NLFs we find for channels 3 and 4. Most of our NLFs are in good agreement with those found by C&S, except for NOAA-09 and TIROS-N. C&S arbitrarily set the TIROS-N NLF to zero[4]. When we evaluate the data, using our diurnal correction, sampling, merging and fitting procedures, except with the NLFs set to C&S's values, we obtain a trend of 0.030 K/decade, much closer C&S's value of 0.015. Alternatively, if we use our NLFs, except that we fix the value of the NOAA-9 NLF to C&S's value of 0.095, we obtain a trend of 0.049 K/decade, indicating that differences in this one NLF is responsible for most of effect of the different NLFs. The remaining difference is likely to be due to differences in our treatments of the diurnal cycle. We have now performed merges for the MSU channels 2,3 and 4, as well as the 19,22, and 37 GHz SSM/I channels using the NLF methodology. In none of these other cases does the absolute value of a NLF exceed 0.03, leading us to suspect the C&S methodology is somehow flawed for NOAA-9.

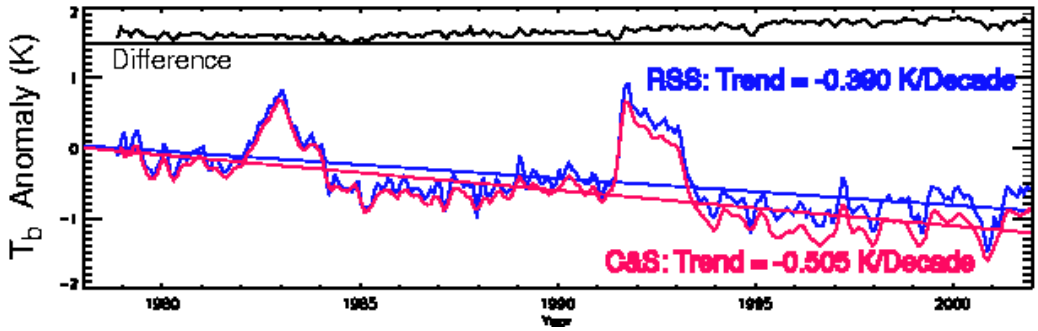

Figure 24. Comparison of MSU Channel 4 global Time series. Our result shows approximately 0.115 K decade less cooling than the C&S results for the same time period.

B. CHANNEL 4

We performed a similar comparison of global time series for MSU channel 4. In Fig. 24, we plot both our global time series we found, and that produced by Christy and Spencer, on the same plot, along with the difference between the time series. The difference is smoothed by a running mean of 3 months to accentuate long-term effects. Our time series shows 0.115 K/decade less cooling than C&S. This is likely to be due to our inclusion of NLFs in our merging procedure, and differences in the diurnal correction. When we repeat the merging process with the NLFs set to zero, and no diurnal correction, we obtain a trend of –0.512 K/decade, and a time series that is virtually identical to C&S's results.

V. Summary and Outlook

We have completed the intersatellite merging process for MSU channels 2, 3 and 4, and produced a climate-quality brightness temperature dataset for use by the scientific community for each of these channels. For both channels 2 and 4 our results show increased warming/ reduced cooling relative to Christy and Spencer. We strongly suspect that these differences are due to different choices for some (channel 2) or all (channel 4) of the non-linearity factors used to adjust the brightness temperatures before merging. Our process for determining these factors is unified and straightforward, giving equal weight to each five-day period of satellite overlap, and does not require a large number of subjective decisions. The biggest source of error in our long-term time series is probably due to errors in our adjustment for diurnal drifts. We plan to further validate model-derived diurnal cycles using a set of radiosonde observations that were made 4 or more time each day.

During the next year we plan to focus on two tasks. First, extend the merging procedure to include data from the AMSU series of instruments. Second, we plan perform the merge for MSU channel 1. In order to do this, we need to refine our surface model, both to remove the diurnal cycle, and to remove the surface temperature trend from the trend in the lower troposphere. We will also investigate inversion methods for removing the stratospheric and surface signals from the MSU channel 2 trends.

REFERENCES

[1] R. W. Spencer and J. R. Christy, "Precise Monitoring of Global Temperature Trends from Satellites," *Science*, vol. 247, pp. 1558-1562, 1990.

[2] J. R. Christy, R. W. Spencer, and E. S. Lobl, "Analysis of the merging procedure for the MSU daily temperature time series," *Journal of Climate*, vol. 11, pp. 2016-2041, 1998.

[3] J. R. Christy, R. W. Spencer, and R. T. McNider, "Reducing Noise in the MSU Daily Lower-Tropospheric Global Temperature Dataset," *Journal of Climate*, vol. 8, pp. 888-896, 1994.

[4] J. R. Christy, R. W. Spencer, and W. D. Braswell, "MSU Tropospheric Temperatures: Dataset Construction and Radiosonde Comparisons," *Journal of Atmospheric and Oceanic Technology*, vol. 17, pp. 1153-1170, 2000.

[5] J. T. Kiehl, J. J. Kack, G. B. Bonan, B. A. Boville, D. L. Williamson, and P. J. Rasch, "The National Center for Atmospheric Research Community Climate Model CCM3,", *Journal of Climate* vol. 6, pp 1131-1149, 1998.

[6] F. J. Wentz, "Algorithm Theoretical Basis Document: AMSR Ocean Algorithm," Remote Sensing Systems, Santa Rosa, CA, RSS Tech. Report 110398, November 3, 1998.

[7] C. L. Gentemann, F. J. Wentz, C. Mears, and D. Smith, "In Situ Validation of TRMM microwave Sea Surface Temperatures," *Unpublished*, 2002.